JACS
JOURNAL OF THE AMERICAN CHEMICAL SOCIETY
Communication
pubs.acs.org/JACS

SERS-Encoded Nanogapped Plasmonic Nanoparticles: Growth of Metallic Nanoshell by Templating Redox-Active Polymer Brushes

Jibin Song,[†] Bo Duan,[†] Chenxu Wang,[†] Jiajing Zhou,[†] Lu Pu,[†] Zheng Fang,[†] Peng Wang,[†,‡] Teik Thye Lim,[‡,§] and Hongwei Duan*,[†]

[†]School of Chemical and Biomedical Engineering, Nanyang Technological University, 70 Nanyang Drive, Singapore 637457
[‡]Nanyang Environment and Water Research Institute (NEWRI), Nanyang Technological University, 1 Cleantech Loop, Singapore 637141
[§]School of Civil and Environmental Engineering, Nanyang Technological University, 50 Nanyang Avenue, Singapore 639798

Supporting Information

ABSTRACT: We report a new strategy to synthesize core−shell metal nanoparticles with an interior, Raman tag-encoded nanogap by taking advantage of nanoparticle-templated self-assembly of amphiphilic block copolymers and localized metal precursor reduction by redox-active polymer brushes. Of particular interest for surface-enhanced Raman scattering (SERS) is that the nanogap size can be tailored flexibly, with the sub-2 nm nanogap leading to the highest SERS enhancement. Our results have further demonstrated that surface functionalization of the nanogapped Au nanoparticles with aptamer targeting ligands allows for specific recognition and ultrasensitive detection of cancer cells. The general applicability of this new synthetic strategy, coupled with recent advances in controlled wet-chemical synthesis of functional nanocrystals, opens new avenues to multifunctional core−shell nanoparticles with integrated optical, electronic, and magnetic properties.

The development of nanostructured probes with unique optical, electronic, and magnetic properties has opened up new possibilities for molecular imaging and spectroscopic detection of specific targets in biomedical and environmental applications.[1] Surface-enhanced Raman scattering (SERS) that allows for detecting fingerprint vibrational spectra of single molecules has emerged as a powerful technique for ultrasensitive detection.[2] Plasmonic metal nanostructures with confined electromagnetic field arising from localized surface plasmon resonance (LSPR) are compelling SERS substrates under intense research.[3] In particular, tight interparticle junctions of plasmonic nanostructures, exhibiting locally enhanced electromagnetic field, have shown dramatically improved signal amplification for Raman molecules at the nanogap area.[3a,4] There is growing interest in compact, nanometer-sized SERS probes with built-in nanogap hotspots, which not only provide fundamental insights into the structure-SERS activity correlation but also can possibly address the practical needs in crossing size-limited biological barriers.[5] Major efforts have been made to develop multimeric ensembles of metal nanostructures with tailored interparticle nanogaps via lithographic and self-assembly approaches.[6] More recently, Nam et al. have reported the use of DNA-functionalized Au nanoparticles to synthesize core−shell SERS nanoprobes with 1 nm interior gap, which show highly uniform and efficient SERS activity in contrast to the anisotropic signal from multimeric ensembles.[7]

Here we report a new class of core−shell Au nanoparticles with a built-in Raman-encoded nanogap that can be tailored in sub-10 nm range. The use of amphiphilic block copolymer, consisting of a Raman dye-tagged hydrophobic block and a hydrophilic block carrying redox-active phenol pedant groups, forms the technological basis of our strategy. As illustrated in Figure 1, self-assembly of amphiphilic block copolymers around Au nanoparticles leads to core−shell hybrid nanoparticles, with the Raman dye-tagged hydrophobic block sandwiched between the Au core and the hydrophilic polymer brush shell. The abundant phenol groups in the shell subsequently reduce Au precursor locally to form an integral Au nanoshell, giving rise to nanogapped nanoparticles (NNPs) with Raman tags positioned

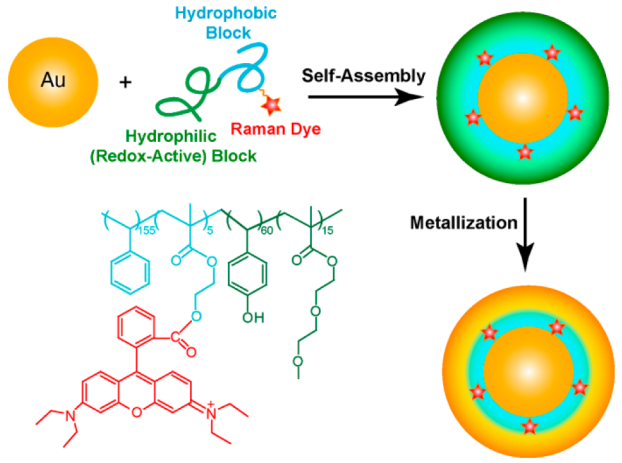

Figure 1. Schematic illustration of the synthesis of nanogapped Au nanoparticles, based on Au nanoparticles templated self-assembly of amphiphilic block copolymers and the localized reduction of Au precursor by phenol group-containing polymer brushes, and chemical structure of the Raman dye-tagged amphiphilic block copolymer.

Received: February 27, 2014
Published: April 28, 2014

dx.doi.org/10.1021/ja502024d | J. Am. Chem. Soc. 2014, 136, 6838−6841

in the nanogap between the Au core and shell. Au nanoshell, as a pioneering class of plasmonic nanostructures, has been explored for a broad spectrum of applications in nanomedicine and biosensing.[8] Conventional synthesis of Au nanoshell involves immobilization of tiny Au nanoparticle seeds on a dielectric or semiconductor core and subsequent electroless Au plating on the seeded nanoparticle for complete shell growth.[9] Our strategy of taking advantage of redox-active polymer coating represents an entirely new approach toward the growth of metallic nanoshell, which coupled with nanoparticle-templated self-assembly of amphiphilic block polymers, provides new opportunities to prepare a diverse range of hybrid core−shell nanostructures with a built-in nanogap. Of particular interest for the development of SERS-encoded plasmonic nanostructures is that this method allows for positioning and locking Raman tags inside the nanogap hotspot, eliminating the possible signal fluctuation resulting from detachment or diffusion that often happens to Raman tags anchored on nanoparticle surfaces. Also important is that controlling the thickness of polymer shell in the block copolymer-coated nanoparticles makes it possible to tailor the core−shell spacing (that is width of the nanogap) of the NNPs for optimized SERS performance. Furthermore, the SERS-encoded NNPs can be easily functionalized with a thiolated aptamer that is specific to cancer biomarker MUC-1 protein,[10] and the bioconjugated nanoparticles lead to specific targeting and ultrasensitive SERS spectroscopic detection of breast cancer cells with overexpressed MUC-1 on their membrane.

The amphiphilic block copolymer (Figure 1) that we synthesized by atom transfer radical polymerization (ATRP) (details in Supporting Information (SI)) consists of hydrophobic polystyrene (PS) block and hydrophilic block of 4-vinylphenol (VPh) and di(ethylene glycol) methyl ether methacrylate (EGM) copolymer (PVPhEGM). Raman probe, rhodamine B (RhB), was tagged on the hydrophobic block by copolymerization of a RhB-containing monomer (Figure 1) and styrene (St). The pedant phenol group of VPh is a strong reducing agent when reaction pH is higher than its pK_a (~10).[11] Its deprotonation at this condition endows PVPhEGM copolymer with excellent water solubility. Our experiments have shown that the characteristic red color of Au nanoparticles immediately appeared upon addition of $KAuCl_4$ into aqueous solution (pH 11) of PVPhEGM copolymer, indicative of strong reducing activity of the phenol group. Transmission electron microscopy (TEM) observation (Figure S1) confirms the generation of Au nanoparticles. Micellization of the amphiphilic block copolymer was induced by adding water, which is a selective solvent for hydrophilic PVPhEGM block, into DMSO solution of the polymer. We have found that it is necessary to have 20% hydrophilic EGM in the PVPhEGM block to give rise to stable micelles. Importantly, the PVPhEGM copolymer in the micelles maintained the strong reducing power. TEM images (Figure S2) display that slowly adding $KAuCl_4$ into the micelle dispersion (pH 11) led to localized reduction of Au precursor on the micelle surface, forming a complete Au nanoshell eventually. It is worthwhile mentioning that localized reduction of Au precursor by PVPhEGM eliminates possible self-nucleation of the precursor in solution to form free nanoparticles, which often occurs when external reducing agents are used.

ATRP allows for optimizing molecular weight and composition of the amphiphilic block copolymer for efficient encapsulation of nanoparticles and Raman probe tagging.[12] The block copolymer with a composition of St_{155}-RhB_5-VPh_{60}-EGM_{15} was selected to coat 20 nm Au nanoparticles synthesized by citrate reduction. Previous work on nanoparticle-templated self-assembly of amphiphilic block copolymers mostly used PS-*b*-poly(acrylic acid) (PAA).[13] Taton et al. reported that thickness of the PS-*b*-PAA coating can be controlled by varying the polymer to nanoparticle ratio, with higher ratio resulting in greater surface density, more stretched polymer chain and thicker coating.[13b] Our results in this study have demonstrated that the block copolymer we designed can also give rise to efficient encapsulation of nanoparticles. As displayed in TEM images (Figure 2a−c), increasing the average

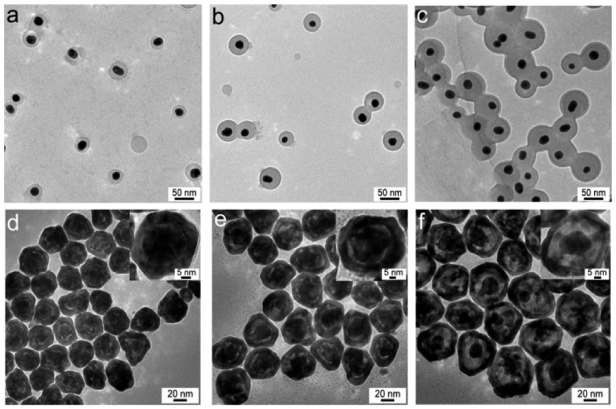

Figure 2. TEM images of polymer-encapsulated gold nanoparticles (20 nm) with different thickness of polymer coating: 11 (a), 18 (b), and 26 nm (c). TEM images of the corresponding Au NNPs with an interior nanogap of 1.5 (d), 5 (e), and 11 nm (f).

number of polymer chains on each nanoparticle from 720, 2000, and 3500 (details in Figures S3 and S4) led to gradually increased thickness for the polymer coating from 11, 18, to 26 nm. Hydrodynamic diameter of the three samples measured by dynamic light scattering is 49, 64, and 81 nm (Figure S5). When the polymer-coated nanoparticles underwent Au deposition by localized reduction of $KAuCl_4$, core−shell nanoparticles with a built-in nanogap were produced (Figures 2d−f and S6). More importantly, control over the polymer thickness in the hybrid nanoparticles was translated into the ability to tailor the nanogap size. For the three hybrid nanoparticles with a polymer thickness of 11, 18, and 26 nm, the nanogap expands from 1.5 ± 0.1, 5 ± 0.7, to 11 ± 1.1 nm (Figure S7). Interestingly, it appears that interconnecting bridges were formed between Au core and shell in the NNPs (insets in Figures 2d−f and S6), suggesting that the RhB-labeled PS block unlike silica coating reported previously[14] did not completely insulate the core nanoparticles from Au deposition. We reason that epitaxial growth of Au on the Au core at defected regions of the polymer coating led to the formation of the nanobridges. Notably, recent report by Nam et al. has suggested that forming nanobridges in the nanogap leads to greatly improved electromagnetic enhancement and consequently better SERS activity.[7]

Optical properties of plasmonic nanostructures are strongly dependent on their structural parameters and immediate dielectric environment.[15] Figure 3a shows that the LSPR of 20 nm Au nanoparticles red-shifted 8−535 nm after coated with the block copolymers because of higher refractive index of the polymer coating, compared to water. The NNPs exhibit significantly different LSPR profile. For the two samples with

dx.doi.org/10.1021/ja502024d | J. Am. Chem. Soc. 2014, 136, 6838−6841

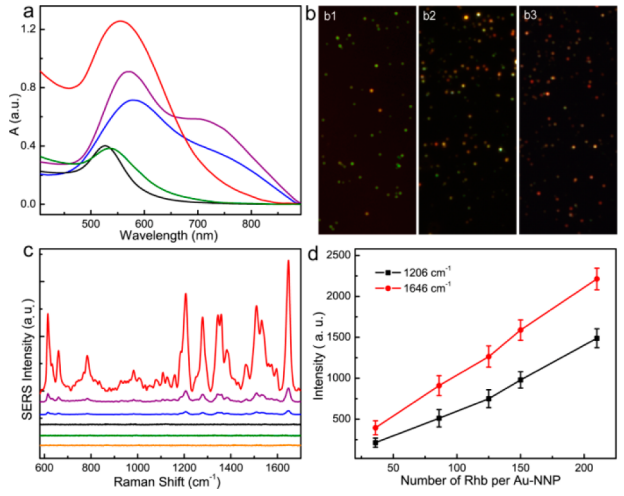

Figure 3. (a) UV−vis spectra of the 20 nm Au nanoparticle (black line), polymer-coated nanoparticle (green line) and Au-NNP with 1.5 nm (red line), 5 nm (purple line) and 11 nm (blue line) nanogap. (b) Dark-field images of Au-NNPs with 1.5 nm gap (b1), 5 nm gap (b2) and 11 nm gap (b3). (c) SERS spectra of Au-NNPs (0.4 nM) with 1.5 nm gap (red line), 5 nm gap (purple line) and 11 nm gap (blue line); 40 nm Au nanoparticle (black line); hollow Au nanoshells (green line), and double-layered Au nanoparticles of ∼43 nm with RhB tags positioned between the two layers (orange line). (d) SERS intensity at 1646 and 1206 cm^{-1} as a function of the average number of RhB molecules loaded in each particle.

larger nanogap (purple and blue lines in Figure 3a), a new resonance component emerged at 730 nm after growth of Au shell, in addition to the peak at lower wavelength. In contrast, when the nanogap shrinks to ∼1.5 nm, LSPR of the NNP resembles that of solid nanoparticles, and only one dipole resonance at 556 nm was detected, which is in line with what reported recently.[7] In comparison with the polymer-coated 20 nm Au nanoparticle core, extinction efficiency of the NNP has increased by a factor of 3.2. Dark-field imaging reveals the scattering property of NNPs at single particle level.[16] As displayed in Figures 3b and S8, the NNP with 1.5 nm interior nanogap predominantly shows green-yellow scattering, and the scattering of NNPs with larger gap red shifts into the orange-red range, which is consistent with the extinction spectra obtained in bulk measurements.

The combinational use of RhB-tagged and RhB-free block copolymer for Au nanoparticle encapsulation allows us to control the average number of Raman probes loaded in the nanogap. As summarized in Figure 3c, SERS measurements (632.8 nm excitation) on the NNP samples containing an average number of 200 RhB in each particle reveal that the NNP with 1.5 nm nanogap shows much better SERS activity compared to the NNP with larger gap sizes. The calculated enhancement factor (EF) of the 1.5 nm gap sample is 1.4×10^8, dropping to 1.1×10^7 and 2.7×10^6 when the gap size increases to 5 and 11 nm. Because the RhB tags residing in the nanogap have no direct contact with the Au surfaces, electromagnetic enhancement is expected to have a leading contribution to the SERS activity of the NNPs, which, in conjugation with the dramatic field enhancement of sub-2 nm nanogap, results in the highest signal intensity of the NNP with 1.5 nm gap. In clear contrast, negligible SERS signal was detected from solid Au nanoparticles of similar size (40 nm), demonstrating the importance of placing Raman tags inside the nanogap hotspots.

The Au nanoshell prepared by localized reduction of Au precursor on the RhB-labeled PS-*b*-PVPhEGM micelles also showed no SERS activity. Co-adsorption of RhB dye and end-thiolated PVPhEGM on 20 nm Au nanoparticles, followed by PVPhEGM-induced Au deposition, gives rise to double-layered Au nanoparticles of ∼43 nm (Figure S9) with RhB tags positioned between the two layers. These nanoparticles, although having roughly the same size as the NNPs, also showed poor SERS amplification. Another strong evidence supporting the major contribution of plasmonic coupling between the Au core and shell is that signal intensity of Raman peaks at 1206 and 1646 cm^{-1} is linearly dependent on the number of RhB probe loaded in the nanogap (Figure 3d).

We next explored the use of NNPs for the specific targeting, Raman imaging, and spectroscopic detection of cancer cells. Breast cancer cell line, MCF-7, is known to have highly overexpressed MUC-1 protein on its cell membrane.[10] The Au NNPs offer straightforward surface functionalization by forming Au−S bond with incoming ligands. Here a MUC-1 aptamer carrying a thiol group at its 5′ end was attached on the NNP with 1.5 nm gap.[17] Dual-modality dark-field and fluorescent imaging clearly shows the efficient binding and uptake of aptamer-conjugated NNPs into the MCF-7 cells. Figure 4a

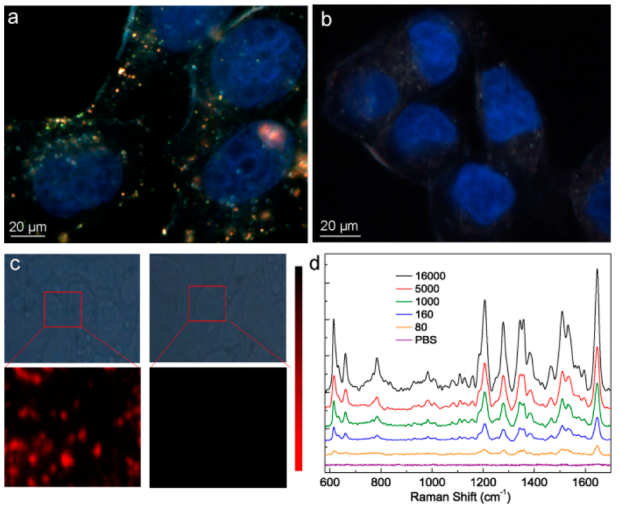

Figure 4. Dark-field imaging of the MCF-7 cells incubated with aptamer-conjugated Au NNPs (a) and Au NNPs modified with scrambled DNA sequence (b). (c) Bright-field (top) and Raman mapping (bottom) of the MCF-7 cells labeled with targeted (left) and nontargeted Au NNPs (right). (d) Raman spectra of different number of MCF-7 cells treated with targeted Au NNPs.

reveals that both green-yellow scattering from single NNPs and orange-colored scattering from small clusters were observed in the live cells. On the other hand, the NNPs modified with a scrambled DNA sequence did not lead to obvious labeling (Figure 4b) of the MCF-7 cells. Raman imaging (Figure 4c), generated by mapping Raman signal at 1646 cm^{-1}, also shows the same trend. While a strong punctuate signal was detected in the cells labeled with the MUC-1 aptamer targeted NNPs, NNPs carrying scrambled DNA sequence did not afford detectible signal. The strong SERS signal of the NNP probe enabled ultrasensitive measurement of the labeled MCF-7 cells. A minimum number of 30 cells/mL (Figures 4d and S10) can be detected for MCF-7 cells incubated with the aptamer-targeted NNPs for 40 min, indicating the potential use of NNP

dx.doi.org/10.1021/ja502024d | J. Am. Chem. Soc. 2014, 136, 6838−6841

probes for detecting circulating tumor cells.[18] The cells treated with the targeted NNP of various concentrations (0.25−2.0 nM) up to 240 min showed more than 95% viability (Figure S11), suggesting the excellent biocompatibility of the Au NNPs.

In summary, we have developed a new synthetic method toward SERS-encoded NNPs based on nanoparticle-templated self-assembly of amphiphilic block copolymers and the use of redox-active polymer carrying phenol groups for localized metal precursor reduction. One key finding is that the nanogap sizes in core−shell NNPs can be readily tailored by controlling the polymer coating thickness, leading to highly SERS-active NNPs with 1.5 nm interior gap for ultrasensitive SERS detection of cancer cells. Our strategy is broadly applicable for other functional nanocrystals, which, in combination with recent advances in wet-chemical synthesis and surface engineering of functional nanocrystals of diverse chemical identity,[19] opens a new avenue for controlled synthesis of multifunctional nanogapped nanocrystals, such as fluorescent quantum dot core-plasmonic metal shell nanoparticles.[1e,20] Likewise, converting the nanoscopic domains of redox-active polymers through localized reduction provides an enabling method for designing metal nanostructures with customized plasmonic and electronic properties.[21]

■ ASSOCIATED CONTENT

Supporting Information

Supporting data and experimental details. This material is available free of charge via the Internet at http://pubs.acs.org.

■ AUTHOR INFORMATION

Corresponding Author

hduan@ntu.edu.sg

Notes

The authors declare no competing financial interest.

■ ACKNOWLEDGMENTS

This work is supported by Ministry of Education-Singapore (MOE) (RGT19/13 and RGT47/13). H.D. thanks the Nanyang Assistant Professorship for financial support. B.D. acknowledges a research scholarship from the SMART program of MOE.

■ REFERENCES

(1) (a) Smith, A. M.; Duan, H. W.; Mohs, A. M.; Nie, S. M. *Adv. Drug Delivery Rev.* **2008**, *60*, 1226. (b) Thakor, A. S.; Jokerst, J.; Zavaleta, C.; Massoud, T. F.; Gambhir, S. S. *Nano Lett.* **2011**, *11*, 4029. (c) Shen, S.; Wang, Q. *Chem. Mater.* **2012**, *25*, 1166. (d) Halas, N. J.; Lal, S.; Link, S.; Chang, W. S.; Natelson, D.; Hafner, J. H.; Nordlander, P. *Adv. Mater.* **2012**, *24*, 4842. (e) Lee, N.; Hyeon, T. *Chem. Soc. Rev.* **2012**, *41*, 2575. (f) Vigderman, L.; Zubarev, E. R. *Adv. Drug Delivery Rev.* **2013**, *65*, 663.

(2) (a) Alvarez-Puebla, R. A.; Liz-Marzán, L. M. *Small* **2010**, *6*, 604. (b) Halvorson, R. A.; Vikesland, P. J. *Environ. Sci. Technol.* **2010**, *44*, 7749. (c) Craig, A. P.; Franca, A. S.; Irudayaraj, J. *Annu. Rev. Food Sci. Technol.* **2013**, *4*, 369.

(3) (a) Camden, J. P.; Dieringer, J. A.; Zhao, J.; Van Duyne, R. P. *Acc. Chem. Res.* **2008**, *41*, 1653. (b) Qian, X. M.; Nie, S. M. *Chem. Soc. Rev.* **2008**, *37*, 912.

(4) (a) Talley, C. E.; Jackson, J. B.; Oubre, C.; Grady, N. K.; Hollars, C. W.; Lane, S. M.; Huser, T. R.; Nordlander, P.; Halas, N. J. *Nano Lett.* **2005**, *5*, 1569. (b) Li, W.; Camargo, P. H. C.; Lu, X.; Xia, Y. *Nano Lett.* **2008**, *9*, 485. (c) Banholzer, M. J.; Millstone, J. E.; Qin, L.; Mirkin, C. A. *Chem. Soc. Rev.* **2008**, *37*, 885. (d) Rycenga, M.; Camargo, P. H. C.; Li, W.; Moran, C. H.; Xia, Y. *J. Phys. Chem. Lett.* **2010**, *1*, 696. (e) Lim, D. K.; Jeon, K. S.; Kim, H. M.; Nam, J. M.; Suh, Y. D. *Nat. Mater.* **2010**, *9*, 60. (f) Yin, J.; Wu, T.; Song, J.; Zhang, Q.; Liu, S.; Xu, R.; Duan, H. *Chem. Mater.* **2011**, *23*, 4756. (g) Lu, W.; Singh, A. K.; Khan, S. A.; Senapati, D.; Yu, H.; Ray, P. C. *J. Am. Chem. Soc.* **2010**, *132*, 18103.

(5) Dvir, T.; Timko, B. P.; Kohane, D. S.; Langer, R. *Nat. Nanotechnol.* **2011**, *6*, 13.

(6) (a) Nie, Z. H.; Fava, D.; Rubinstein, M.; Kumacheva, E. *J. Am. Chem. Soc.* **2008**, *130*, 3683. (b) Chen, G.; Wang, Y.; Yang, M.; Xu, J.; Goh, S. J.; Pan, M.; Chen, H. *J. Am. Chem. Soc.* **2010**, *132*, 3644. (c) Wustholz, K. L.; Henry, A. I.; McMahon, J. M.; Freeman, R. G.; Valley, N.; Piotti, M. E.; Natan, M. J.; Schatz, G. C.; Duyne, R. P. V. *J. Am. Chem. Soc.* **2010**, *132*, 10903. (d) Alvarez-Puebla, R. A.; Agarwal, A.; Manna, P.; Khanal, B. P.; Aldeanueva-Potel, P.; Carbó-Argibay, E.; Pazos-Pérez, N.; Vigderman, L.; Zubarev, E. R.; Kotov, N. A.; Liz-Marzán, L. M. *Proc. Natl. Acad. Sci. U. S. A.* **2011**, *108*, 8157. (e) Shen, X.; Chen, L.; Li, D.; Zhu, L.; Wang, H.; Liu, C.; Wang, Y.; Xiong, Q.; Chen, H. *ACS Nano* **2011**, *5*, 8426. (f) Osberg, K. D.; Rycenga, M.; Harris, N.; Schmucker, A. L.; Langille, M. R.; Schatz, G. C.; Mirkin, C. A. *Nano Lett.* **2012**, *12*, 3828. (g) Cheng, L.; Song, J.; Yin, J.; Duan, H. *J. Phys. Chem. Lett.* **2011**, *2*, 2258. (h) Hu, K. W.; Liu, T. M.; Chung, K. Y.; Huang, K. S.; Hsieh, C. T.; Sun, C. K.; Yeh, C. S. *J. Am. Chem. Soc.* **2009**, *131*, 14186. (I) Gao, B.; Gaurav, A.; Tao, A. R. *Nat. Nanotechnol.* **2012**, *7*, 433.

(7) Lim, D. K.; Jeon, K. S.; Hwang, J. H.; Kim, H.; Kwon, S.; Suh, Y. D.; Nam, J. M. *Nat. Nano.* **2011**, *6*, 452.

(8) Wang, H.; Brandl, D. W.; Nordlander, P.; Halas, N. J. *Acc. Chem. Res.* **2006**, *40*, 53.

(9) (a) Oldenburg, S. J.; Averitt, R. D.; Westcott, S. L.; Halas, N. J. *Chem. Phys. Lett.* **1998**, *288*, 243. (b) Bardhan, R.; Grady, N. K.; Ali, T.; Halas, N. J. *ACS Nano* **2010**, *4*, 6169. (c) Zubarev, E. R. *Nat. Nanotechnol.* **2013**, *8*, 396.

(10) (a) Wu, P.; Gao, Y.; Zhang, H.; Cai, C. *Anal. Chem.* **2012**, *84*, 7692. (b) Hu, Y.; Duan, J.; Zhan, Q.; Wang, F.; Lu, X.; Yang, X. D. *PLoS One* **2012**, *7*, e31970.

(11) Xie, J.; Zheng, Y.; Ying, J. Y. *J. Am. Chem. Soc.* **2009**, *131*, 888.

(12) Matyjaszewski, K.; Xia, J. *Chem. Rev.* **2001**, *101*, 2921.

(13) (a) Kang, Y.; Taton, T. A. *Angew. Chem., Int. Ed.* **2005**, *44*, 409. (b) Kang, Y.; Taton, T. A. *Macromolecules* **2005**, *38*, 6115. (c) Chen, T.; Yang, M.; Wang, X.; Tan, L. H.; Chen, H. *J. Am. Chem. Soc.* **2008**, *130*, 11858. (d) Chen, T.; Wang, H.; Chen, G.; Wang, Y.; Feng, Y.; Teo, W. S.; Wu, T.; Chen, H. *ACS Nano* **2010**, *4*, 3087.

(14) (a) Xia, X. H.; Liu, Y.; Backman, V.; Ameer, G. A. *Nanotechnology* **2006**, *17*, 5435. (b) Bardhan, R.; Mukherjee, S.; Mirin, N. A.; Levit, S. D.; Nordlander, P.; Halas, N. J. *J. Phys. Chem. C* **2009**, *114*, 7378.

(15) (a) Jain, P. K.; Huang, X.; El-Sayed, I. H.; El-Sayed, M. A. *Acc. Chem. Res.* **2008**, *41*, 1578. (b) Anker, J. N.; Hall, W. P.; Lyandres, O.; Shah, N. C.; Zhao, J.; Van Duyne, R. P. *Nat. Mater.* **2008**, *7*, 442.

(16) (a) Raschke, G.; Kowarik, S.; Franzl, T.; Sönnichsen, C.; Klar, T. A.; Feldmann, J.; Nichtl, A.; Kürzinger, K. *Nano Lett.* **2003**, *3*, 935. (b) Song, J.; Zhou, J.; Duan, H. *J. Am. Chem. Soc.* **2012**, *134*, 13458.

(17) (a) Nam, J. M.; Thaxton, C. S.; Mirkin, C. A. *Science* **2003**, *301*, 1884. (b) Wang, C.; Du, Y.; Wu, Q.; Xuan, S.; Zhou, J.; Song, J.; Shao, F.; Duan, H. *Chem. Commun.* **2013**, *49*, 5739.

(18) Wang, X.; Qian, X. M.; Beitler, J. J.; Chen, Z. G.; Khuri, F. R.; Lewis, M. M.; Shin, H. J. C.; Nie, S. M.; Shin, D. M. *Cancer Res.* **2011**, *71*, 1526.

(19) (a) Park, J.; An, K.; Hwang, Y.; Park, J. G.; Noh, H. J.; Kim, J. Y.; Park, J. H.; Hwang, N. M.; Hyeon, T. *Nat. Mater.* **2004**, *3*, 891. (b) Cheng, L.; Liu, A. P.; Peng, S.; Duan, H. W. *ACS Nano* **2010**, *4*, 6098. (c) Smith, A. M.; Nie, S. M. *Acc. Chem. Res.* **2010**, *43*, 190. (d) Song, J.; Pu, L.; Zhou, J.; Duan, B.; Duan, H. *ACS Nano* **2013**, *7*, 9947.

(20) (a) Jin, Y.; Gao, X. *Nat. Nanotechnol.* **2009**, *4*, 571. (b) Ho, D.; Sun, X.; Sun, S. *Acc. Chem. Res.* **2011**, *44*, 875.

(21) Pang, X.; Zhao, L.; Han, W.; Xin, X.; Lin, Z. *Nat. Nanotechnol.* **2013**, *8*, 426.